

Tunable correlation in twisted monolayer-trilayer graphene

Dongdong Ding(丁冬冬), Ruirui Niu(牛锐锐), Xiangyan Han(韩香岩), Zhuangzhuang Qu(曲壮壮), Zhiyu Wang(王知雨), Zhuoxian Li(李卓贤), Qianling Liu(刘倩伶), Chunrui Han(韩春蕊), and Jianming Lu(路建明)
Citation: Chin. Phys. B, 2023, 32 (**6**): 067204. DOI: 10.1088/1674-1056/acc8c3
Journal homepage: http://cpb.iphy.ac.cn; http://iopscience.iop.org/cpb

What follows is a list of articles you may be interested in

Long-range adsorbate interactions mediated by two-dimensional Dirac fermions

Xiaohui Wang(王晓慧), Zhen-Guo Fu(付振国), Zhigang Wang(王志刚), Feng Chi(迟锋), and Ping Zhang(张平)
Chin. Phys. B, 2023, 32 (**5**): 057201. DOI: 10.1088/1674-1056/acae77

Correlated states in alternating twisted bilayer-monolayer-monolayer graphene heterostructure

Ruirui Niu(牛锐锐), Xiangyan Han(韩香岩), Zhuangzhuang Qu(曲壮壮), Zhiyu Wang(王知雨), Zhuoxian Li(李卓贤), Qianling Liu(刘倩伶), Chunrui Han(韩春蕊), and Jianming Lu(路建明)
Chin. Phys. B, 2023, 32 (**1**): 017202. DOI: 10.1088/1674-1056/ac9de4

Observation of quadratic magnetoresistance in twisted double bilayer graphene

Yanbang Chu(褚衍邦), Le Liu(刘乐), Yiru Ji(季怡汝), Jinpeng Tian(田金朋), Fanfan Wu(吴帆帆), Jian Tang(汤建), Yalong Yuan(袁亚龙), Yanchong Zhao(赵岩翀), Xiaozhou Zan(昝晓州), Rong Yang(杨蓉), Kenji Watanabe, Takashi Taniguchi, Dongxia Shi(时东霞), Wei Yang(杨威), and Guangyu Zhang(张广宇)
Chin. Phys. B, 2022, 31 (**10**): 107201. DOI: 10.1088/1674-1056/ac6866

Tunable valley filter efficiency by spin-orbit coupling in silicene nanoconstrictions

Yi-Jian Shi(施一剑), Yuan-Chun Wang(王园春), and Peng-Jun Wang(汪鹏君)
Chin. Phys. B, 2021, 30 (**5**): 057201. DOI: 10.1088/1674-1056/abcf35

Magnetotransport properties of graphene layers decorated with colloid quantum dots

Ri-Jia Zhu(朱日佳), Yu-Qing Huang(黄雨青), Jia-Yu Li(李佳玉), Ning Kang(康宁), Hong-Qi Xu(徐洪起)
Chin. Phys. B, 2019, 28 (**6**): 067201. DOI: 10.1088/1674-1056/28/6/067201

RAPID COMMUNICATION

Tunable correlation in twisted monolayer–trilayer graphene

Dongdong Ding(丁冬冬)[1], Ruirui Niu(牛锐锐)[1], Xiangyan Han(韩香岩)[1], Zhuangzhuang Qu(曲壮壮)[1], Zhiyu Wang(王知雨)[1], Zhuoxian Li(李卓贤)[1], Qianling Liu(刘倩伶)[1], Chunrui Han(韩春蕊)[2,3,‡], and Jianming Lu(路建明)[1,†]

[1] *State Key Laboratory for Mesoscopic Physics, School of Physics, Peking University, Beijing* 100871, *China*
[2] *Institute of Microelectronics, Chinese Academy of Sciences, Beijing* 100029, *China*
[3] *University of Chinese Academy of Sciences, Beijing* 100049, *China*

(Received 6 February 2023; revised manuscript received 28 March 2023; accepted manuscript online 30 March 2023)

Flat-band physics of moiré superlattices, originally discovered in the celebrated twisted bilayer graphene, have recently been intensively explored in multilayer graphene systems that can be further controlled by electric field. In this work, we experimentally find the evidence of correlated insulators at half filling of the electron moiré band of twisted monolayer–trilayer graphene with a twist angle around 1.2°. Van Hove singularity (VHS), manifested as enhanced resistance and zero Hall voltage, is observed to be distinct in conduction and valence flat bands. It also depends on the direction and magnitude of the displacement fields, consistent with the asymmetric crystal structure. While the resistance ridges at VHS can be enhanced by magnetic fields, when they cross commensurate fillings of the moiré superlattice in the conduction band, the enhancement is so strong that signatures of correlated insulator appear, which may further develop into an energy gap depending on the correlation strength. At last, Fermi velocity derived from temperature coefficients of resistivity is compared between conduction and valence bands with different displacement fields. It is found that electronic correlation has a negative dependence on the Fermi velocity, which in turn could be used to quantify the correlation strength.

Keywords: twisted multilayer graphene heterostructure, correlated states, van Hove singularity

PACS: 72.80.Vp, 73.40.–c, 73.21.Cd **DOI:** 10.1088/1674-1056/acc8c3

1. Introduction

Electronic correlation and topology, two important topics in condensed matter physics, meet in twisted van der Waals heterostructures. In the celebrated prototype – twisted bilayer graphene (TBG), fruitful quantum phenomena have been observed, such as superconductivity, (fractional) quantum anomalous Hall effect, and correlated insulator states.[1–19] The key here is the flat bands induced by interlayer moiré potential, giving rise to strong correlation that can be characterized by non-negligible Coulomb repulsion U and exchange interaction.[20] Combined with extremely high density of states (DOS) ρ at van Hove singularity, the Stoner criterion ($\rho U > 1$) can be meet, leading to symmetry breaking of the otherwise degenerate spin, valley and sublattice flavors,[21–31] thus topologically nontrivial bands may be observed. Note that, there are also topologically trivial states competing for the ground state. To win the energy competition, various methods are introduced, including magnetic field,[4,11,12] substrates with staggered sublattice potential,[8] spin–orbit interaction,[32] twist angle,[33] etc. In addition, to *in situ* control the topological property, displacement field is brought in to tune the essential factors,[9,16,18,19,30,34–39] i.e., band flatness and VHS. For instances, both in twisted monolayer–bilayer graphene[9,19,34,35] and double bilayer graphene,[16–18,30] the bandwidth is observed to depend on not only the conduction/valence band but also the displacement filed; furthermore, VHS is also highly tunable by the displacement field and twist angles. In the former, valley polarization could be achieved at odd number of commensurate fillings that results in quantum anomalous Hall effect,[9,19,35] whereas in the latter spin polarization is found at half filling the moiré band.[16–18,30] Such a flexible field tuning of twisted multilayer graphene motivates us to extensively explore more types of twisted graphene heterostructures beyond the most fundamental TBG.

In this work, we experimentally characterize the phase diagram of twisted monolayer–trilayer graphene. Van Hove singularity is observed in both conduction and valence flat bands, whose positions depend on the displacement fields. It also enhances resistance, and the enhancement grows stronger in magnetic fields. When it crosses commensurate filling points in the conduction band, signatures of correlated insulator appear, and may develop into an energy gap depending on the correlation strength. To quantify the correlation, the Fermi velocity derived from the temperature coefficients of resistivity is compared between the conduction and valence bands with different displacement fields. The negative relationship can be used as an indicator for more novel multilayer graphene heterostructures.

†Corresponding author. E-mail: jmlu@pku.edu.cn
‡Corresponding author. E-mail: hanchunrui@ime.ac.cn

© 2023 Chinese Physical Society and IOP Publishing Ltd

2. Results

Figure 1(a) shows a schematic of the twisted device, in which a trilayer graphene is stacked onto a monolayer graphene with an angle of $\theta \sim 1.2°$, and the top and bottom gates are made of gold and multilayer graphene, respectively. In experiments, the monolayer (enclosed by red dashed lines in Fig. 1(b)) and Bernal trilayer graphene (blue dashed lines, with its Raman spectrum shown in the right inset) were precut from a single graphene flake, then picked up by a hexagonal boron nitride (BN) crystal sequentially and finally put onto another BN and a long and thin graphite flake. Standard e-beam lithography was used to pattern the heterostructure and the finished device with indexed electrodes is displayed in the inset of Fig. 1(b). To determine the twist angle, we measured Hall density $n_{\rm H} = -B/(eR_{xy})$ as a function of gate voltages, and extracted the capacitance of he top and bottom gates. Since we know the gate voltage corresponding to the full filling of the first and second moiré bands, it can be immediately translated to the carrier density for full filling of the moiré superlattice $n_{\rm s}$. Then the twisted angle θ can be calculated by

$$n_{\rm s} = \frac{4}{A} \approx \frac{8\theta^2}{\sqrt{3}a^2}, \tag{1}$$

where A is the area of a superlattice unit cell, $a = 0.246$ nm is the lattice constant of graphene. To check the homogeneity of the twist sample, we measured the electronic phase diagram across both pins 1–19 (Fig. 1(c)) and 11–13 (Fig. 1(d)) as a function of carrier density and displacement field D. Here the carrier density n has been converted into filling factor ν, following the formula $\nu = 4n/n_{\rm s}$; D is defined by $D = (D_{\rm b} - D_{\rm t})/2$, where $D_{\rm b(t)} = \varepsilon_0\varepsilon_{\rm b(t)}V_{\rm b(t)}/d_{\rm b(t)}$, $\varepsilon_{\rm b(t)}$ and $d_{\rm b(t)}$ are the dielectric constant and thickness of the bottom (top) dielectric layers. Two phase diagrams are almost identical, with similar features at charge neutral point (CNP, i.e., $\nu = 0$), half ($\nu = 2$) and full ($\nu = 4$) fillings, indicating that the angle disorder is minimized over the whole sample. Nevertheless, the absolute resistance in Fig. 1(d) is relatively small, suggesting that the moiré gaps are smeared by some disorders. Consequently, in the following we focus on the sample between pins 1 and 19 (Fig. 1(c)).

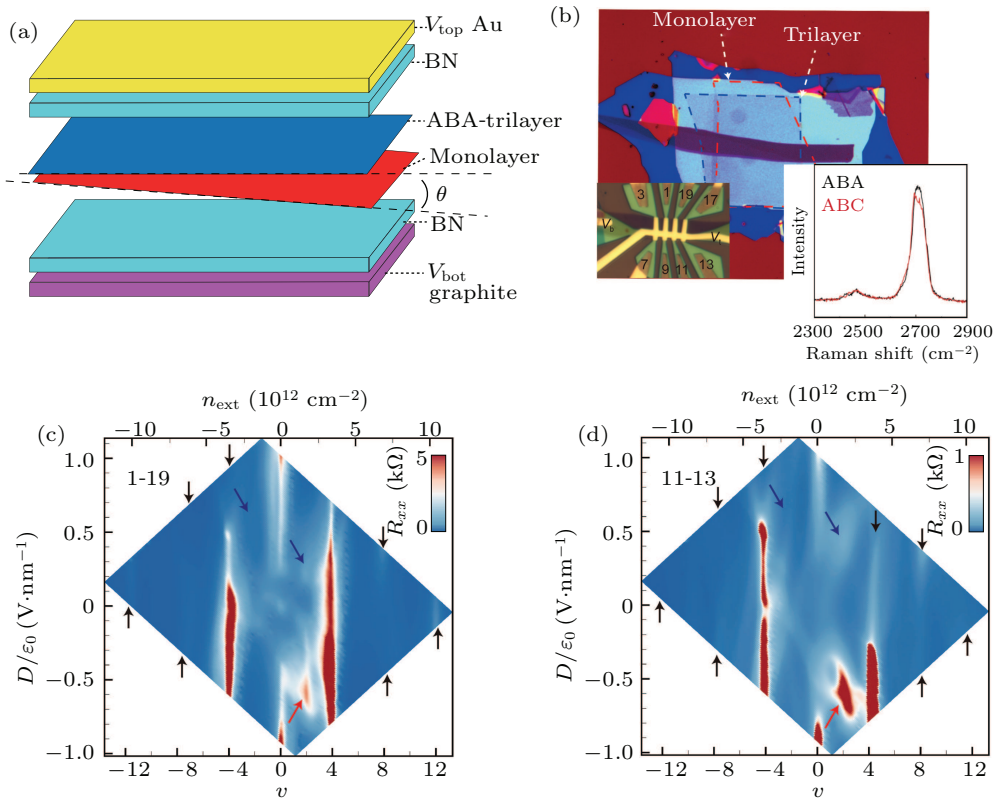


Fig. 1. Electronic phase diagram of the twisted monolayer–trilayer graphene heterostructure. (a) Schematic of the device with the twist angle θ, where the top and bottom gates are metal and a thin graphite, respectively. (b) Optical characterization with enhanced visibility. Left inset: finished device with indexed electrodes. Right inset: Raman spectra of both Bernal and rhombohedral trilayer graphene. (c) Phase diagram as a function of filling factor ν and displacement field D for the sample between pins 1 and 19. (d) Similar phase diagram for the sample between pins 11 and 13.

The most significant features in Fig. 1(c) are electric-field tuned resistive peaks at $\nu = 0$, 2, ± 4 and the asymmetry between positive and negative D. Since the trilayer graphene has a different electronic band structure from monolayer, it is easily understood intuitively that the asymmetric monolayer–trilayer graphene heterostructure relies on the perpendicular electric field: a positive D would lower the electrostatic potential energy of electron carriers residing closer to the bot-

tom monolayer graphene, while a negative D plays an opposite role. That the correlated insulator at $\nu = 2$ only takes place at negative D suggests that the reconstructed band structure indeed has a narrower bandwidth when electrons are more localized in the trilayer part. Moreover, it resides in the conduction flat band but is absent in the valence band. Both characteristics share the similar behavior with that of the aforementioned twisted (monolayer or bilayer)–bilayer systems. This is not surprising, since in the viewpoint of band structure the twisted monolayer–trilayer graphene (denoted as A–ABA) is equivalent to the sum of a twisted monolayer–bilayer graphene and a monolayer graphene (i.e., A–AB+A).[40] Nevertheless, the additional 'equivalent monolayer' is more dispersive, making the electrons less correlated in the twisted monolayer–trilayer graphene than that of the twisted monolayer–bilayer graphene.

Besides the above features, there are some less prominent resistance peaks (white colored in Figs. 1(c) and 1(d) and highlighted by arrows), including straight lines at large integer fillings $\nu = 8$ and 12, and arc-shaped curves at non-integer fillings. For the former, it means the superlattice modulation remains effective to generate multiple moiré bands at high energy, though the bandwidth is not as narrow as that in the vicinity of CNP. For the latter, the white arcs are thinner in the valence band, but greatly broadened in the conduction band. Actually, it spreads into a strip between $\nu = 0$ and 4. Whenever such a strip goes across an integer filling $\nu = 2$, correlated insulators start to develop (red arrow in Fig. 1(c)): while the correlation insulator is obvious at $D < 0$, only a faint white dot is observed at $D > 0$ (black arrow), consistent with the inherent asymmetry.

To probe the origin of these features, we applied various magnetic fields along the perpendicular direction. Figures 2(a) and 2(b) show the longitudinal and Hall resistances at $B = 1$ T, respectively. Compared with the zero-field phase diagrams in Figs. 1(c) and 1(d), the resistance ridges (represented by white strips) become sharper for $-4 < \nu < 4$ and start to be visible for $4 < \nu < 8$. Correspondingly, we observe at exactly the same locations zero Hall resistance (white color) in Fig. 2(b). It can be categorized into two types: one stands for band gaps at integer $\nu = 0, \pm4, \pm8, 12$; the other is for van Hove singularity at non-integer fillings, e.g., $-4 < \nu < 0$, $0 < \nu < 4$ and $4 < \nu < 8$. In particular, around $D \sim -0.6$ V·nm^{-1} and $\nu = 2$ the white strip is severely distorted by the appearance of symmetry-breaking correlated insulators. To better visualize the correspondence between resistance ridges in Fig. 2(a) and zero Hall resistance in Fig. 2(b), line cuts at $D = 0.22$ V·nm^{-1} (upper) and -0.62 V·nm^{-1} (lower) are plotted in Fig. 2(c). Indeed, whenever the red curve crosses the zero line – either due to the energy band gaps or van Hove singularities – there is a resistance peak appearing in the blue curve.

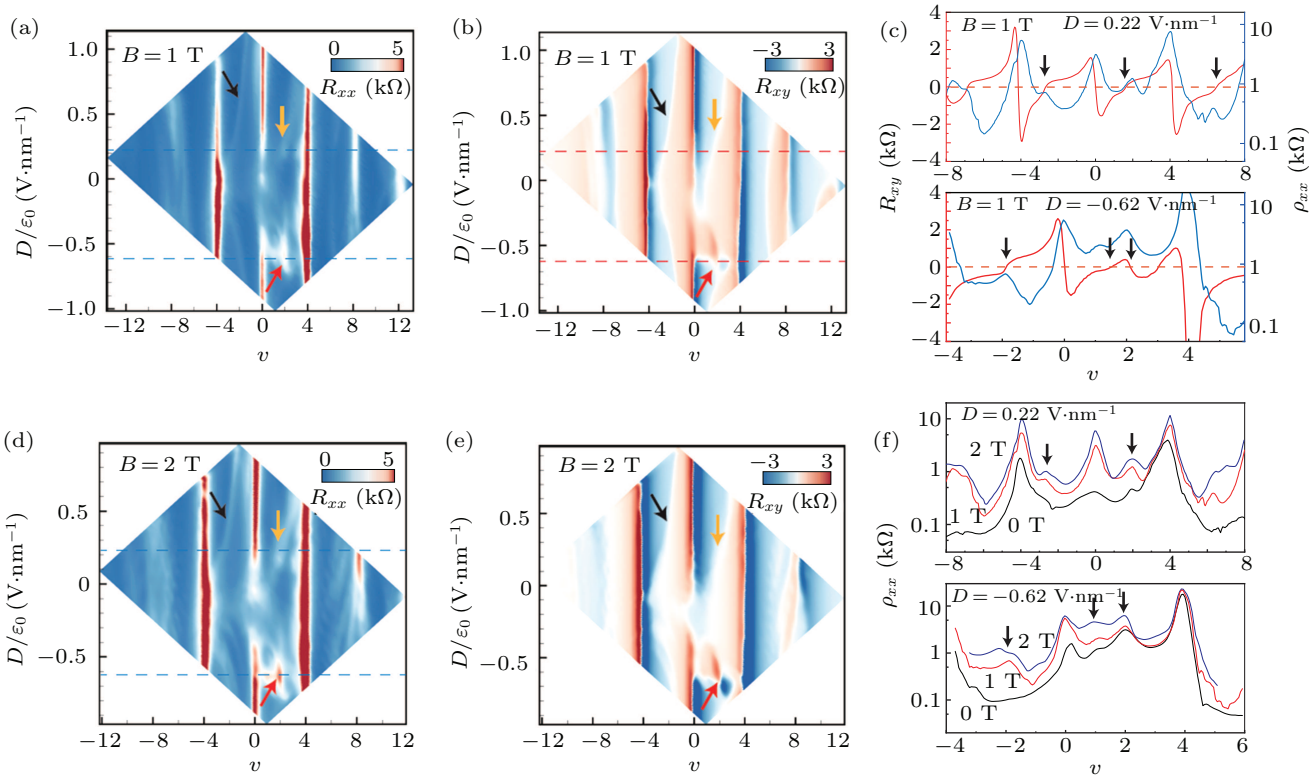


Fig. 2. Magnetic-field enhancement of tunable van Hove singularity. Longitudinal (a) and Hall (b) resistances measured at perpendicular magnetic field $B = 1$ T. Zero Hall resistance in (b) can be categorized into two types. One corresponds to band gaps at integer $\nu = 0, \pm4, \pm8, 12$. The other is van Hove singularity at non-integer fillings, which corresponds to white curves of resistance ridges in (a). (c) To better visualize the correspondence between resistance peaks in (a) and zero Hall resistance in (b), line cuts at $D = 0.22$ V·nm^{-1} (upper) and -0.62 V·nm^{-1} (lower) are plotted. Longitudinal (d) and Hall (e) resistances measured at $B = 2$ T. Besides the increased resistance peaks along van Hove singularity in a large magnetic field, significant enhancement is found for correlated insulators at $\nu = 2$ and $D \sim -0.5$ V·nm^{-1} (d) with clear symmetry breaking. (f) The enhancement of resistance by perpendicular B fields is more clearly presented in line cuts at $D = 0.22$ V·nm^{-1} (upper) and -0.62 V·nm^{-1} (lower).

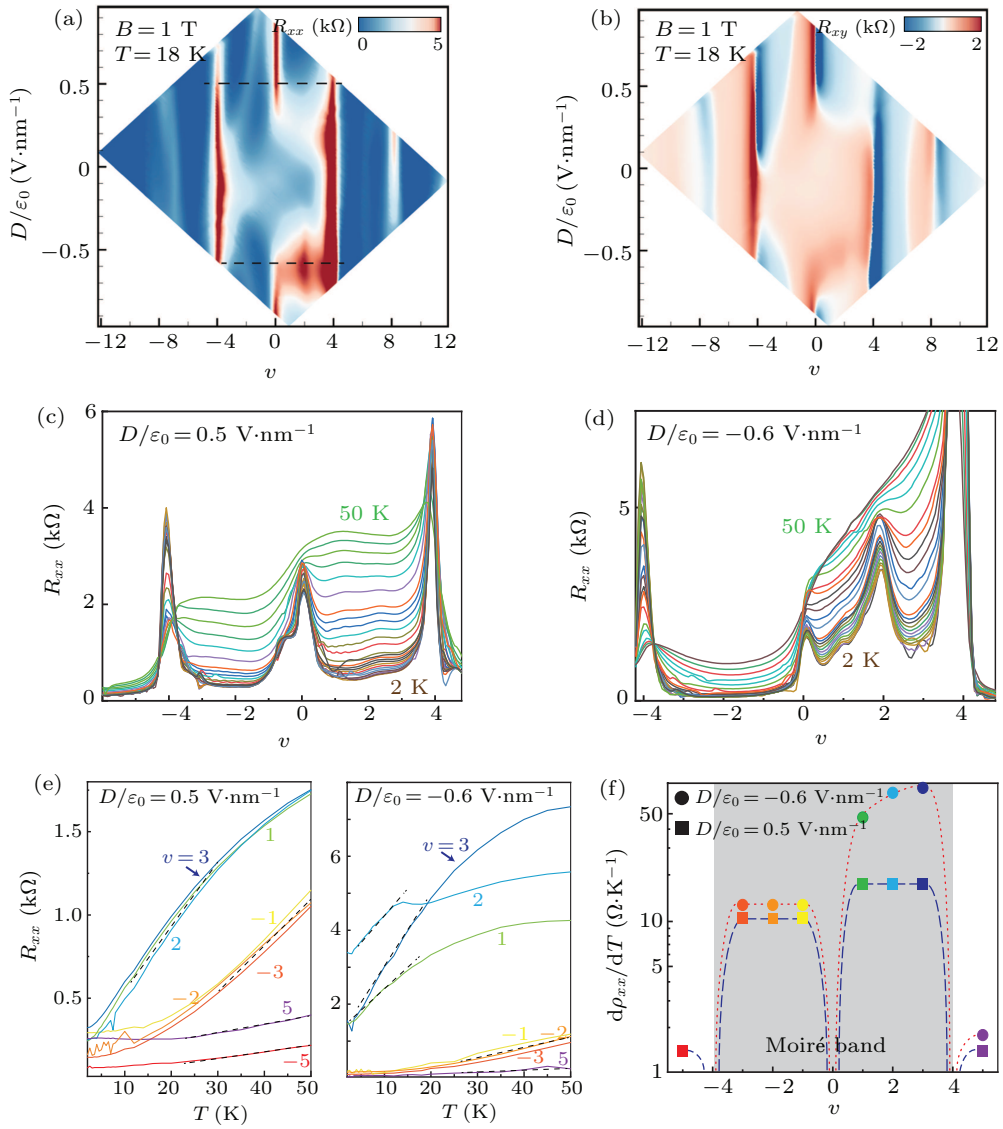


Fig. 3. Enhanced electron–phonon scattering in a flat band. (a), (b) Longitudinal and Hall resistances measured at 18 K. Transfer curves at $D = 0.5$ V·nm^{-1} (c) and -0.6 V·nm^{-1} (d) at various temperatures from 50 K to 2 K. (e) Temperature dependent resistance at various filling factors (denoted by arrows in (c) and (d)). (f) Characteristics of slopes derived by dashed lines in (e) (and converted to resistivity ρ_{xx}) are summarized. Within the flat band, the slope is more than one order larger than that in the dispersive bands.

The magnetic field enhancement of resistance ridges is interesting, encouraging us to apply a large field to examine the behavior. Figures 2(d) and 2(e) show the longitudinal and Hall resistances measured at $B = 2$ T. Compared with the performance at 1 T, significant enhancement is found for the correlated insulators at $\nu = 1$, 2 and $D \sim -0.5$ V·nm^{-1}. In particular, the sign reversal of Hall effect at $\nu = 2$ indicates clear symmetry breaking of isospin flavors. Besides that, the resistance peak along van Hove singularity indeed grows with increasing magnetic fields. For clarity, we put linecuts of two displacement fields at various magnetic fields in Fig. 2(f). In the upper panel ($D = 0.22$ V·nm^{-1}), systematic evolution is clearly seen at $\nu \sim -2.5$, and 2 (denoted by arrows). Similarly for $D = -0.62$ V·nm^{-1} in the lower panel, the field enhancement is observed at $\nu \sim -2$, 1, and 2 (denoted by arrows).

We would like to stress that, although VHS is important to enhance DOS and hence electronic correlation, the other essential factor for electronic correlation is the band flatness, or roughly the reciprocal of the bandwidth. Usually, the effective mass $m^* = \hbar^2/\frac{d^2E}{dk^2}$ derived from Shubnikov–de Haas oscillation is taken to evaluate the band flatness in relatively dispersive systems. In a flat-band system with heavy m^*, however, the quantum oscillation magnitude is severely reduced, hindering a quantitative characterization. Instead, recently the Fermi velocity $v_F = \frac{1}{\hbar}\frac{dE}{dk}$ is found to have a strong correlation with electronic correlation.[41,42] Indeed, over the whole Brillion zone Δk is $2\pi/\lambda$ with λ as the length of a unit cell and the bandwidth is ΔE, thus the ratio $\Delta E/\Delta k$ roughly reflects the band flatness. As is well known, v_F can be experimentally obtained by measuring the temperature dependent resistivity through a relation that reads[43–47]

$$\rho = \frac{\pi D_A^2 F}{2 g_s g_v e^2 \hbar \rho_m v_{ph}^2 v_F^2} k_B T, \tag{2}$$

where $D_A = 25$ eV is the acoustic phonon deformation potential, $F \sim 1$ is the form factor accounting for electron–phonon scattering details that differ from monolayer graphene, g_s (g_v) $= 2$ is the spin (valley) degeneracy, e is the elementary charge, $\hbar$ is the reduced Plank constant, $\rho_m = 7.6 \times 10^{-7}$ kg/m^2, and phonon velocity $v_{ph} = 2.1 \times 10^4$ m/s. Take monolayer graphene as an example, $v_F \sim 1 \times 10^6$ m/s leads to the temperature coefficient in the order of 0.1 Ω/K. In a flat band system, v_F will be significantly suppressed, resulting in a substantial temperature coefficient following Eq. (2).

In the twisted monolayer–trilayer graphene, one can deduce from Fig. 2 that, qualitatively, the correlation is strongest in the range of $0 < \nu < 4$ for $D < 0$ and weaker for $D > 0$. As for $-4 < \nu < 0$, both $+/-D$ are too weak to observe correlated features. Now we aim to quantify the correlation by characterizing the temperature dependence of resistivity. Firstly, we check the consistency of phase diagrams at high temperatures. A typical one is taken at 18 K, where $B = 1$ T is applied to examine VHS lines (Fig. 3(a)) and the Hall effect (Fig. 3(b)). Consistent with the low-temperature phase diagrams, all features of interest survive though a little smeared by thermal fluctuation. Then, $D = 0.5$ V/nm (Fig. 3(c)) and -0.6 V/nm (Fig. 3(d)) are selected for measuring temperature dependence of resistivity. Surprisingly, apart from the correlated features ($\nu = 2$, $D = -0.6$ V/nm) and bandgaps ($\nu = 0$, ± 4), the resistance seems to be a plateau in a wide range of carrier filling factors. Consequently, the temperature coefficient should be around a constant within this range, which is derived in Fig. 3(e) and confirmed in Fig. 3(f). It is interesting to find that the coefficient is highest in the range of $0 < \nu < 4$; it is smaller in $-4 < \nu < 0$ and smallest in $|\nu| > 4$. It is also evident that even in the same range $0 < \nu < 4$, the coefficient is much larger for $D < 0$ than $D > 0$. Such a performance perfectly coincides with electronic correlation that inversely connects to the bandwidth.

It is interesting to compare our results with that in twisted graphene systems. For TBG, the coefficient reaches the order of 100 Ω/K when the electronic correlation is maximized at the magic angle.[41] In twisted double bilayer graphene, it also increases fast when approaching the "halo", the regime where the VHS line meets commensurate fillings.[42] Overall, the temperature coefficient can be taken as a convenient method to evaluate the correlation strength in a system in which both correlated gap and SdH oscillation are absent.

3. Conclusion

In twisted monolayer–trilayer graphene, we find that van Hove singularity as well as bandwidth asymmetrically depends on both displacement fields and conduction/valence bands. Therefore, it is highly tunable for electronic correlation and the induced correlated insulators at commensurate fillings. Recently, multilayer graphene[48] (e.g., Bernal trilayer) has been proposed to be a constituent for constructing multiple flat bands in alternating twisted graphene heterostructures (i.e., monolayer–multilayer–monolayer), which is expected to exhibit stronger correlation due to the much higher density of states on the Fermi surface. Our work, as a starting point, thus provides a fundamental understanding of multilayer graphene in twisted graphene, and is believed to encourage more exciting exploration towards this research direction.

Acknowledgements

J. L. acknowledges support from the National Natural Science Foundation of China (Grant No. 11974027), the National Key R&D Program of China (Grant Nos. 2019YFA0307800 and 2021YFA1400100), and Beijing Natural Science Foundation (Grant No. Z190011). C. H. acknowledges support from the National Natural Science Foundation of China (Grant No. 62275265) and Beijing Natural Science Foundation (Grant No. 4222084).

References

[1] Cao Y, Fatemi V, Fang S, Watanabe K, Taniguchi T, Kaxiras E and Jarillo-Herrero P 2018 *Nature* **556** 43
[2] Yankowitz M, Chen S, Polshyn H, Zhang Y, Watanabe K, Taniguchi T, Graf D, Young A F and Dean C R 2019 *Science* **363** 1059
[3] Lu X, Stepanov P, Yang W, Xie M, Aamir M A, Das I, Urgell C, Watanabe K, Taniguchi T, Zhang G, Bachtold A, MacDonald A H and Efetov D K 2019 *Nature* **574** 653
[4] Stepanov P, Das I, Lu X, Fahimniya A, Watanabe K, Taniguchi T, Koppens F H L, Lischner J, Levitov L and Efetov D K 2020 *Nature* **583** 375
[5] Saito Y, Ge J, Watanabe K, Taniguchi T and Young A F 2020 *Nat. Phys.* **16** 926
[6] Liu X, Wang Z, Watanabe K, Taniguchi T, Vafek O and Li J I A 2021 *Science* **371** 1261
[7] Sharpe A L, Fox E J, Barnard A W, Finney J, Watanabe K, Taniguchi T, Kastner M A and Goldhaber-Gordon D 2019 *Science* **365** 605
[8] Serlin M, Tschirhart C L, Polshyn H, Zhang Y, Zhu J, Watanabe K, Taniguchi T, Balents L and Young A F 2020 *Science* **367** 900
[9] Polshyn H, Zhu J, Kumar M A, Zhang Y, Yang F, Tschirhart C L, Serlin M, Watanabe K, Taniguchi T, MacDonald A H and Young A F 2020 *Nature* **588** 66
[10] Nuckolls K P, Oh M, Wong D, Lian B, Watanabe K, Taniguchi T, Bernevig B A and Yazdani A 2020 *Nature* **588** 610
[11] Wu S, Zhang Z, Watanabe K, Taniguchi T and Andrei E Y 2021 *Nat. Mater.* **20** 488
[12] Das I, Lu X, Herzog-Arbeitman J, Song Z D, Watanabe K, Taniguchi T, Bernevig B A and Efetov D K 2021 *Nat. Phys.* **17** 710
[13] Pierce A T, Xie Y, Park J M, Khalaf E, Lee S H, Cao Y, Parker D E, Forrester P R, Chen S, Watanabe K, Taniguchi T, Vishwanath A, Jarillo-Herrero P and Yacoby A 2021 *Nat. Phys.* **17** 1210
[14] Xie Y, Pierce A T, Park J M, Parker D E, Khalaf E, Ledwith P, Cao Y, Lee S H, Chen S, Forrester P R, Watanabe K, Taniguchi T, Vishwanath A, Jarillo-Herrero P and Yacoby A 2021 *Nature* **600** 439
[15] Cao Y, Fatemi V, Demir A, Fang S, Tomarken S L, Luo J Y, Sanchez-Yamagishi J D, Watanabe K, Taniguchi T, Kaxiras E, Ashoori R C and Jarillo-Herrero P 2018 *Nature* **556** 80
[16] Shen C, Chu Y, Wu Q, Li N, Wang S, Zhao Y, Tang J, Liu J, Tian J, Watanabe K, Taniguchi T, Yang R, Meng Z Y, Shi D, Yazyev O V and Zhang G 2020 *Nat. Phys.* **16** 520

[17] Liu X, Hao Z, Khalaf E, Lee J Y, Ronen Y, Yoo H, Haei Najafabadi D, Watanabe K, Taniguchi T, Vishwanath A and Kim P 2020 *Nature* **583** 221

[18] Cao Y, Rodan-Legrain D, Rubies-Bigorda O, Park J M, Watanabe K, Taniguchi T and Jarillo-Herrero P 2020 *Nature* **583** 215

[19] Chen S, He M, Zhang Y H, Hsieh V, Fei Z, Watanabe K, Taniguchi T, Cobden D H, Xu X, Dean C R and Yankowitz M 2021 *Nat. Phys.* **17** 374

[20] Andrei E Y and MacDonald A H 2020 *Nat. Mater.* **19** 1265

[21] Park J M, Cao Y, Watanabe K, Taniguchi T and Jarillo-Herrero P 2021 *Nature* **592** 43

[22] Zondiner U, Rozen A, Rodan-Legrain D, Cao Y, Queiroz R, Taniguchi T, Watanabe K, Oreg Y, von Oppen F, Stern A, Berg E, Jarillo-Herrero P and Ilani S 2020 *Nature* **582** 203

[23] Rozen A, Park J M, Zondiner U, Cao Y, Rodan-Legrain D, Taniguchi T, Watanabe K, Oreg Y, Stern A, Berg E, Jarillo-Herrero P and Ilani S 2021 *Nature* **592** 214

[24] Saito Y, Yang F, Ge J, Liu X, Taniguchi T, Watanabe K, Li J I A, Berg E and Young A F 2021 *Nature* **592** 220

[25] Liu X, Zhang N J, Watanabe K, Taniguchi T and Li J I A 2022 *Nat. Phys.* **18** 522

[26] Zhou H, Xie T, Ghazaryan A, Holder T, Ehrets J R, Spanton E M, Taniguchi T, Watanabe K, Berg E, Serbyn M and Young A F 2021 *Nature* **598** 429

[27] de la Barrera S C, Aronson S, Zheng Z, Watanabe K, Taniguchi T, Ma Q, Jarillo-Herrero P and Ashoori R 2022 *Nat. Phys.* **18** 771

[28] Seiler A M, Geisenhof F R, Winterer F, Watanabe K, Taniguchi T, Xu T, Zhang F and Weitz R T 2022 *Nature* **608** 298

[29] Zhou H, Holleis L, Saito Y, Cohen L, Huynh W, Patterson C L, Yang F, Taniguchi T, Watanabe K and Young A F 2022 *Science* **375** 774

[30] Liu L, Zhang S, Chu Y, Shen C, Huang Y, Yuan Y, Tian J, Tang J, Ji Y, Yang R, Watanabe K, Taniguchi T, Shi D, Liu J, Yang W and Zhang G 2022 *Nat. Commun.* **13** 3292

[31] Jiang Y, Lai X, Watanabe K, Taniguchi T, Haule K, Mao J and Andrei E Y 2019 *Nature* **573** 91

[32] Lin J X, Zhang Y H, Morissette E, Wang Z, Liu S, Rhodes D, Watanabe K, Taniguchi T, Hone J and Li J I A 2022 *Science* **375** 437

[33] Tseng C C, Ma X, Liu Z, Watanabe K, Taniguchi T, Chu J H and Yankowitz M 2022 *Nat. Phys.* **18** 1038

[34] Xu S, Al Ezzi M M, Balakrishnan N, Garcia-Ruiz A, Tsim B, Mullan C, Barrier J, Xin N, Piot B A, Taniguchi T, Watanabe K, Carvalho A, Mishchenko A, Geim A K, Fal'ko V I, Adam S, Neto A H C, Novoselov K S and Shi Y 2021 *Nat. Phys.* **17** 619

[35] He M, Zhang Y H, Li Y, Fei Z, Watanabe K, Taniguchi T, Xu X and Yankowitz M 2021 *Nat. Commun.* **12** 4727

[36] Park J M, Cao Y, Watanabe K, Taniguchi T and Jarillo-Herrero P 2021 *Nature* **590** 249

[37] Cao Y, Park J M, Watanabe K, Taniguchi T and Jarillo-Herrero P 2021 *Nature* **595** 526

[38] Hao Z, Zimmerman A M, Ledwith P, Khalaf E, Najafabadi D H, Watanabe K, Taniguchi T, Vishwanath A and Kim P 2021 *Science* **371** 1133

[39] Niu R, Han X, Qu Z, Wang Z, Li Z, Liu Q, Han C and Lu J 2023 *Chin. Phys. B* **32** 017202

[40] Xie B, Peng R, Zhang S and Liu J 2022 *npj Comput. Mater.* **8** 1

[41] Polshyn H, Yankowitz M, Chen S, Zhang Y, Watanabe K, Taniguchi T, Dean C R and Young A F 2019 *Nat. Phys.* **15** 1011

[42] Chu Y, Liu L, Shen C, Tian J, Tang J, Zhao Y, Liu J, Yuan Y, Ji Y, Yang R, Watanabe K, Taniguchi T, Shi D, Wu F, Yang W and Zhang G 2022 *Phys. Rev. B* **106** 035107

[43] Wu F, Hwang E and Das Sarma S 2019 *Phys. Rev. B* **99** 165112

[44] Li X, Wu F and Das Sarma S 2020 *Phys. Rev. B* **101** 245436

[45] Chen J-H, Jang C, Xiao S, Ishigami M and Fuhrer M S 2008 *Nat. Nanotech.* **3** 206

[46] Dean C R, Young A F, Meric I, Lee C, Wang L, Sorgenfrei S, Watanabe K, Taniguchi T, Kim P, Shepard K L and Hone J 2010 *Nat. Nanotech.* **5** 722

[47] Hwang E H and Das Sarma S 2008 *Phys. Rev. B* **77** 115449

[48] Ma Z, Li S, Lu M, Xu D H, Gao J H and Xie X 2022 *Sci. China Phys. Mech. Astron.* **66** 227211